Electrochemical Oxidative Adsorption of Ethanethiolate on Ag(111)

David W. Hatchett, Keith J. Stevenson, William B. Lacy, Joel M. Harris,* and Henry S. White*

Contribution from the Department of Chemistry, Henry Eyring Building, University of Utah, Salt Lake City, Utah 84112

Received December 23, 1996[⊗]

Abstract: The electrochemical deposition of ethanethiolate monolayers on Ag(111) has been investigated by *in-situ* surface-enhanced Raman spectroscopy (SERS), electrochemical quartz crystal microbalance (EQCM), and voltammetric methods. In aqueous 0.2 M NaOH solutions containing 5 mM ethanethiolate, the voltammetric response at Ag(111) displays two well-resolved surface waves with half-wave potentials ($E_{1/2}$) of −1.17 and −0.95 V vs Ag/AgCl. The two-wave voltammetric response suggests a mechanism of monolayer deposition that consists of two energetically-distinct reaction steps, a conclusion supported by *in-situ* SERS and EQCM measurements of the potential-dependent adsorption isotherm. The voltammetric wave located at more negative potentials ($E_{1/2} = -1.17$ V) has a nearly ideal Nernstian shape and is associated with the initial rapid oxidative adsorption of ethanethiolate at submonolayer coverage. The second wave at more positive potentials ($E_{1/2} = -0.95$ V) corresponds to additional, but kinetically slower, oxidative adsorption of ethanethiolate resulting in an essentially complete monolayer ($\sim 7.8 \times 10^{-10}$ mol/cm^2). The slower kinetics associated with this wave, as well as general features of the wave shape, suggest that structural ordering of the monolayer occurs during the second oxidation. A thermodynamic expression for the dependence of $E_{1/2}$ on the bulk solution concentration of ethanethiolate is derived and employed to determine the number of electrons transferred, $n = 1.06 \pm 0.06$, per molecule of ethanethiolate adsorbed on the Ag(111) surface. A value of $n = 0.90 \pm 0.14$ has also been independently determined by EQCM and coulometric measurements of the mass adsorbed and electrical charge consumed, respectively, during monolayer deposition.

Introduction

Self-assembled monolayers (SAMs) of alkanethiols on Au(111)[1] and other metal surfaces[2] serve as a model system in developing organic synthetic methods for controlling interfacial properties.[3,4] A consensus among researchers working in this field is that self-assembly involves *oxidative adsorption* of the molecule to form a metal−thiolate surface bond, the overall reaction being frequently expressed as eq 1.[2a,4a,5]

$$\mathrm{Au(111) + RSH \rightarrow Au(111)/-SR + {}^1/_2H_2} \qquad (1)$$

While the structure and applications of well-ordered, alkanethiol-based SAMs have been extensively detailed, a number of interesting questions remain unanswered regarding the fundamental mechanistic aspects of monolayer formation. For example, although the rate of self-assembly of well-ordered monolayers in both the vapor and liquid phase has been measured,[1a,5c] very little is known about intermediate surface structures involved in the formation of ordered monolayers. An exception is the recent seminal report by Poirier and Pylant in which the mechanism for the self-assembly of alkanethiol monolayers on Au(111) surfaces in vacuum is reported.[6] On the basis of scanning tunneling microscopy (STM) images obtained at different alkanethiol coverages (controlled by varying the amount of alkanethiol deposited from the gas phase), these researchers unequivocally demonstrated that monolayer formation in the gas phase proceeds through several distinct structural phases that coincide with specific surface coverages. To our knowledge, no similar detailed account of intermediate surface structures exists for self-assembly from the solution phase. In addition, and somewhat remarkably, there does not appear to be any quantitative measurement of the thermodynamic stability of alkanethiolate monolayers in contact with liquids (aqueous or otherwise).

The oxidative adsorption of thiols in electrochemical experiments has been described by several researchers, beginning with the very early report of Kolthoff and Barnum.[7] Stankovich and Bard reported voltammetric studies of the oxidative adsorption of cysteine at Hg electrodes, demonstrating that compact monolayers of thiols can be deposited by electrochemical methods.[8] In a 1992 report, Weisshaar, Lamp, and Porter communicated a preliminary description of the electrochemical

[⊗] Abstract published in *Advance ACS Abstracts,* July 1, 1997.

(1) (a) Bain, C. D.; Troughton, E. B.; Tao, Y-T.; Evall, J.; Whitesides, G. M.; Nuzzo, R. G. *J. Am. Chem. Soc.* **1989**, *111*, 321. (b) Porter, M. D.; Bright, T. B.; Allara, D. L.; Chidsey, C. E. D. *J. Am. Chem. Soc.* **1987**, *109*, 3559. (c) Bain, C. D.; Evall, J.; Whitesides, G. M. *J. Am. Chem. Soc.* **1989**, *111*, 7155. (d) Stole, S. M.; Porter, M. C. *Langmuir* **1990**, *6*, 1199. (e) Atre, S. V.; Liedberg, B.; Allara, D. L. *Langmuir* **1995**, *11*, 3992. (f) Thomas, R. C.; Sun, L.; Crooks, R. M. *Langmuir* **1991**, *7*, 620.

(2) (a) Laibinis, P. E.; Whitesides, G. M.; Allara, D. L.; Tao, Y.-T.; Parikh, A. N.; Nuzzo, R. G. *J. Am. Chem. Soc.* **1991**, *113*, 7152. (b) Sellers, H.; Ulman, A.; Shnidman, Y.; Eilers, J. E. *J. Am. Chem. Soc.* **1993**, *115*, 9389. (c) Richardson, J. N.; Peck, S. R.; Curtin, L. S.; Tender, L. M.; Terrill, R. H.; Carter, M. T.; Murray, R. W.; Rowe, G. K.; Creager, S. E. *J. Phys. Chem.* **1995**, *99*, 766.

(3) (a) Dubios, L. H.; Nuzzo, R. G. *Annu. Rev. Phys. Chem.* **1992**, *43*, 437. (b) Mirkin, C. A.; Ratner, M. A. *Annu. Rev. Phys. Chem.* **1992**, *43*, 719. (c) Thomas, R. C.; Sun, L.; Crooks, R. M.; Ricco, A. J. *Langmuir* **1991**, *7*, 620. (d) Bain, C. D.; Whitesides, G. M. *J. Am. Chem. Soc.* **1989**, *111*, 7164. (e) Laibinis, P. E.; Bain, C. D.; Nuzzo, R. G.; Whitesides, G. M. *J. Phys. Chem.* **1995**, *99*, 7663.

(4) (a) Ulman, A.; Eilers, J. E.; Tillman, N. *Langmuir* **1989**, *5*, 1147. (b) Evans, S. D.; Ulman, A. *Chem. Phys. Lett.* **1990**, *170*, 462.

(5) (a) Nuzzo, R. G.; Fusco, F. A.; Allara, D. L. *J. Am. Chem. Soc.* **1987**, *109*, 2358. (b) Nuzzo, R. G.; Dubois, L. H.; Allara, D. L. *J. Am. Chem. Soc.* **1990**, *112*, 558. (c) Chailapakul, O.; Sun, L.; Xu, C.; Crooks, R. M. *J. Am. Chem. Soc.* **1993**, *115*, 12459.

(6) (a) Poirier, G. E.; Pylant, E. D. *Science* **1996**, *272*, 1145. (b) Poirier, G. E.; Tarlov, M. J. *J. Phys. Chem.* **1995**, *99*, 10966.

(7) (a) Kolthoff, I. M.; Barnum, C. *J. Am. Chem. Soc.* **1940**, *62*, 3061. (b) Lee, W. *Biochem. J.* **1971**, *121*, 563.

(8) Stankovich, M. T.; Bard, A. J. *J. Electroanal. Chem.* **1977**, *75*, 487.

S0002-7863(96)04396-X CCC: $14.00

deposition of alkanethiolate monolayers on Au(111) in ethanolic solutions.[9] Specifically, these researchers reported the *reversible* voltammetric deposition of monolayers in solutions containing alkanethiolates and showed that electrochemically deposited monolayers (e.g., dodecanethiolate and hexanethiolate monolayers) have structures and interfacial characteristics essentially identical to those of SAMs prepared by spontaneous adsorption of the corresponding alkanethiol from ethanolic solutions at open circuit. The voltammetric response of Au(111) electrodes in contact with alkanethiolate solutions displays a single, well-resolved wave, corresponding to oxidative adsorption of the alkanethiolate (eq 2).

$$\mathrm{Au(111)} + \mathrm{RS^-} \rightleftharpoons \mathrm{Au(111)/-SR^{(\lambda-1)}} + \lambda \mathrm{e^-} \qquad (2)$$

Equation 2 represents the "half-cell" oxidative reaction occurring during the spontaneous self-assembly of alkanethiols (eq 1) (the charge balance of the overall reaction is maintained by reduction of the protons and/or solvent). The quantity λ is the degree of the charge transferred between the alkanethiolate and the surface and is indicative of the strength of the Au−S bond. For RS^- adsorption, λ is anticipated to have a value between 0 and 1. The total quantity of charge transferred per molecule of adsorbed alkanethiolate, *n*, however, comprises both the faradaic charge transferred in forming the Au−S surface bond (λ), as well as any electrical charge associated with purely physical processes that occur during monolayer deposition (e.g., reorientation of solvent dipoles). It is not necessary or anticipated that λ will be equal in magnitude to *n*, a point that has been recently addressed by Schneider and Buttry[10a] and by Majda and co-workers.[10b] The relationship between λ and *n* is of concern in the present paper, because the deposition of an alkanethiolate monolayer may significantly alter the structure of the metal/solution interface. Of more general interest is that the *reversible* redox reaction expressed in eq 2 suggests the use of electrochemical methods to investigate the mechanism of self-assembly. In addition, and as shown in this paper, the voltammetric measurement of the reversible redox potential associated with eq 2 provides a simple experimental means of assessing the thermodynamic stability of alkanethiolate-based SAMs, a methodology that, to our knowledge, has yet to be employed.

In previous papers, we have described the reversible oxidative adsorption of hydrosulfide (HS^-) on Ag(111) in aqueous solutions (pH = 13).[11] HS^- represents the $n_c = 0$ structure in the alkanethiolate series, $C_{n_c}H_{2n_c+1}S^-$. The voltammetric response of highly-oriented Ag(111) surfaces is sufficiently well-resolved in HS^- solutions that characteristic surface waves associated with the formation of intermediate Ag−SH and Ag_2S monolayer structures are observable prior to bulk oxidation of the Ag electrode. Voltammetric half-wave potentials measured in these experiments provide a direct measure of the thermodynamic stability of the intermediate surface structures. More recently, we have extended these studies to alkanethiolates (n_c = 2−8, 10) and have observed that the electrochemical response at Ag(111) also displays well-resolved *reversible* voltammetric waves associated with the deposition of alkanethiolate monolayers.[12]

In this paper, we demonstrate that the electrochemical formation of ethanethiolate ($CH_3CH_2S^-$) monolayers on highly-oriented Ag(111) surfaces proceeds through a multistep mechanism involving at least two energetically-distinct surface phases that are thermodynamically stable at different $CH_3CH_2S^-$ coverages. Our conclusion is based on electrochemical data and supported by *in-situ* surface-enhanced Raman spectroscopy (SERS) and quartz crystal microbalance measurements (EQCM) of the potential-dependent adsorption of $CH_3CH_2S^-$. We further demonstrate that thermodynamic parameters characterizing the stability of the intermediate and final monolayer structures, as well the number of electrons transferred, *n*, can be determined in a relatively straightforward manner using voltammetric methods.

Experimental Section

Sample Preparation. Highly-oriented Ag(111) films were epitaxially grown on muscovite mica using a Veeco CVC CVE-20 filament evaporator (TFS Technologies, Albuquerque, NM). Freshly-cleaved mica samples (~3 cm^2) were placed in a stainless steel substrate holder, positioned ~20 cm above a resistively-heated Mo boat containing Ag shot (99.999%, Alpha/Aesar). A movable shutter separated the evaporation boat and mica samples. The evaporation chamber was kept at a base pressure between 8×10^{-7} and 2×10^{-6} Torr using sorption and turbomolecular pumps.

The mica was heated prior to deposition of Ag using backside illumination from two quartz lamps to 250 °C for 1 h to desorb surface impurities. The temperature was monitored using a type K thermocouple sandwiched between two sheets of mica and mounted on the substrate holder. The Ag shot was resistively heated in a Mo boat for 2 min with the shutter closed to outgas impurities in the metal. The shutter was then opened, and Ag was allowed to deposit onto the mica at a rate of 0.2 nm/s, until a film thickness of 300 nm was achieved. The Ag films were then annealed at 250 °C for 6 h using the quartz lamp heaters. The evaporation chamber was vented to atmosphere, and the samples were immediately placed in a desiccator filled with N_2 prior to the electrochemical experiments. X-ray photoelectron spectroscopy did not reveal any adsorbed oxygen on the Ag surface. Scanning tunneling microscopy and glancing angle X-ray crystallographic diffraction measurements[13] indicate that the thermally annealed Ag films have a high degree of (111) orientation and are atomically smooth with terrace widths on the order of ~100 nm. Unannealed Ag films were produced in the same manner, with the following modifications. The mica substrates were not heated before or after deposition of Ag, and a deposition rate of ~1 nm/s was employed.

The underpotential deposition (upd) of Pb on the Ag(111) electrodes was used to determine electrochemically-active electrode areas and surface roughness factors (RF = electrochemically active area/geometrical area).[13,14] The upd of Pb at Ag(111) electrodes prepared in this laboratory, and the determination of RF values, has been previously detailed.[13] RF values were determined to be 1.02 ± 0.04 and 1.16 ± 0.06 for the annealed and unannealed Ag(111) films, respectively (based on independent measurements on 30 annealed and 17 unannealed Ag(111) film electrodes).

Polycrystalline Ag electrodes used in the *in-situ* SERS experiments were prepared by melting the end of a 1 mm diameter Ag wire (Alpha/Aesar, 99.999% pure) in an H_2 flame to form a sphere. A Cu lead was fused to the Ag wire using an H_2/O_2 flame. The Ag sphere and Cu wire were encased in molten Pyrex and allowed to cool. The end of the assembly was sanded with 400 grit sandpaper until an ~2 mm diameter Ag disk was exposed. The Ag disk was mechanically polished to a mirror finish with successively smaller sizes (1.5 to 0.01 μm) of Al_2O_3 powder (Alpha/Aesar), washed with triply distilled water, and

(9) Weisshaar, D. E.; Lamp, B. D.; Porter, M. D. *J. Am. Chem. Soc.* **1992**, *114*, 5860.

(10) (a) Schneider, T. W.; Buttry, D. A. *J. Am. Chem. Soc.* **1993**, *115*, 12391. (b) Krysinski, P.; Chamberlain, R. V., II; Majda, M. *Langmuir* **1994**, *10*, 4286.

(11) (a) Hatchett, D. W.; Gao, X.; Catron, S. W.; White, H. S. *J. Phys. Chem.* **1996**, *100*, 331. (b) Hatchett, D. W.; White, H. S. *J. Phys. Chem.* **1996,** *100*, 9854. (c) Stevenson, K. J.; Hatchett, D. W.; White, H. S. *J. Isr. Chem.* Submitted.

(12) Hatchett, D. W.; Stevenson; K. J.; Harris, J. M.; White, H. S. Manuscript in preparation.

(13) Stevenson, K. J.; Hatchett, D. W.; White H. S. *Langmuir* **1996**, *12*, 494.

(14) (a) Bewick, A.; Thomas, B. *J. Electroanal. Chem.* **1976**, *70*, 239. (b) Bewick, A.; Thomas, B. *J. Electroanal. Chem.* **1977**, *84*, 127.

sonicated in methanol. Prior to SERS measurements, the Ag disk electrode was roughened by oxidation−reduction cycling (ORC) in the presence of KCl, while illuminating the surface with a 50 mW argon ion laser.[15]

Materials and Electrochemical Apparatus. A standard one-compartment, three-electrode cell, equipped with inlet and outlet ports for N_2 flow, was used for all electrochemical experiments unless noted otherwise. Pt wire and Ag/AgCl (3 M NaCl) electrodes were used as the counter and reference electrodes, respectively. Solutions were purged for ∼20 min with N_2 to remove O_2 from the solution, and a positive pressure of N_2 was maintained over the solution during measurements. All measurements were made at 25 ± 2 °C.

The mica/Ag(111) electrodes were partially immersed in the solution, defining active areas between 0.1 and 0.75 cm^2. Areas were determined after removal of the electrode from solution by measuring the length of the electrode wetted by the solution (the wetted area is readily determined by visual inspection of the electrode). Voltammetric data were obtained using a Princeton Applied Research Corp. (PARC) model 173 potentiostat and a model 175 Universal programmer. A Kipp and Zonen model BD-90 x-y recorder was used to record voltammetric curves.

All solutions were prepared using water obtained from a Barnstead "E-pure" water purification system. NaOH (Mallinckrodt), KCl (Mallinckrodt), PbO (J. T. Baker, 99%), and CH_3CH_2SH (Aldrich, 99%) were reagent grade and used as received.

Electrochemical Quartz Crystal Microbalance (EQCM). The EQCM used in this investigation is similar to the instrument described by Ward.[16] The electrode areas for the voltammetric and frequency response were 0.399 and 0.178 cm^2, respectively. A homemade oscillator circuit was used to drive the crystal at its fundamental resonant frequency (5 MHz). The frequency and current were monitored at ∼0.5 s intervals with a Hewlett Packard 5384A frequency counter and a Keithley 195A digital multimeter, interfaced with a Macintosh Centris 650 computer. A complete description of the instrument and detection limits have been reported previously.[11a]

Electrochemical Scanning Tunneling Microscopy (ESTM). The microscope and control electronics were custom built and similar to that described elsewhere.[17] A three-electrode electrochemical cell, machined out of Kel-F, containing a Pt wire counter electrode and a Ag wire reference electrode was employed. All STM measurements were made under potential control. The microscope is covered with a glass bell jar, modified with a N_2 gas inlet, to provide an O_2-free atmosphere. Mechanically-cut Pt(90%)-Rh(10%) tips were used in all imaging experiments. The STM tips were insulated with Apiezon wax to reduce faradaic reactions.[18]

Spectroscopic Conditions and Instrumentation for Surface-Enhanced Raman Scattering. A detailed description of the Raman instrument used for the SERS measurements has been described previously.[19] Incoherent plasma lines in the laser beam were eliminated by a combination of two Pellin-Brocha prisms (Optics for Research, ABDU-20), a variable aperture, a plano convex lens (f = 500 mm, Newport Corp.), a 0.5 mm pinhole, and a second variable aperture.

SERS measurements using unannealed mica/Ag electrodes at open circuit were performed with the samples immersed in a glass cuvette (Type 3 with 5 polished windows, 20 × 10 × 45 mm^3, NSG Precision Cells, Inc.). The beam was focused to a 75 μm wide × 2 mm long stripe on the samples with a cylindrical lens (f = 75 mm, Newport Corp.) rather than a circular spot, to reduce the power density of the incident beam in order to minimize sample heating. *In-situ* measurements using the ORC-roughened polycrystalline Ag disk under active potential control were performed in a three-electrode cell, with the electrode surface oriented at 60° relative to the incident radiation.

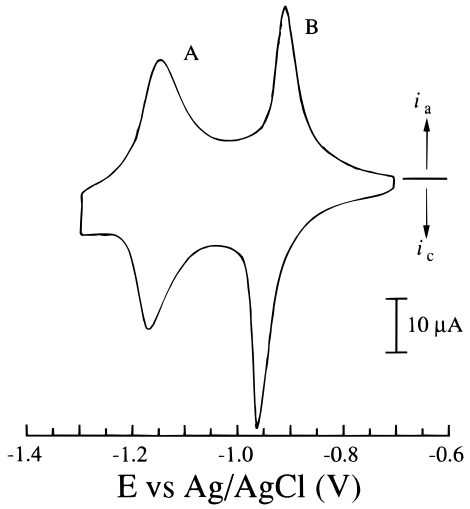

Figure 1. Voltammetric response of an annealed Ag(111) electrode (area = 0.41 cm^2) in 0.2 M NaOH solution containing 5 mM $CH_3CH_2S^-$. Scan rate = 100 mV/s.

All spectra were obtained at a monochromator setting calibrated in the EG&G PARC software by fitting the frequencies of several Raman bands of pyridine in the 400−1100 cm^{-1} region to a second-order polynomial. s-Polarized irradiation was employed in experiments using the ORC-roughened Ag disk; p-polarized light was employed for measurements using the mica/Ag samples. The choices of polarization were governed only by the scattering sensitivity for the two substrates.[20]

Results and Discussion

Voltammetric Measurement of the Oxidative Adsorption of Ethanethiolate. The steady-state voltammetric response of a 6 h thermally annealed Ag(111) electrode in aqueous 0.2 M NaOH solution containing 5 mM CH_3CH_2SH is presented in Figure 1. The primary sulfur species present in solution is $CH_3CH_2S^-$ (99.82%), based on the estimated pK_a of CH_3CH_2-SH (∼10.6).[21] Two well-resolved waves (labeled A and B) are observed, with half-wave potentials, $E_{1/2}$, of −1.17 and −0.95 V ($E_{1/2} = (E_{pc} + E_{pa})/2$, where E_{pc} and E_{pa} are the cathodic and anodic peak potentials, respectively). Wave A is symmetrical with a small peak splitting, $\Delta E_p = (E_{pa} - E_{pc}) \approx 5$ mV at 100 mV/s, indicative of a reversible surface redox process.[22] Wave B displays a larger, scan-rate-dependent peak splitting ($\Delta E_p \approx$ 40 mV at 100 mV/s), suggestive of a kinetically slow reaction. In the following sections, we present results of *in-situ* SERS and EQCM experiments that demonstrate that both waves A and B correspond to $CH_3CH_2S^-$ adsorption at the Ag(111) surface, eq 3. The two-wave voltammetric response suggests that $CH_3CH_2S^-$ deposition occurs by a mechanism involving at least two energetically-distinct surface phases.

$$\mathrm{Ag(111) + CH_3CH_2S^- \rightleftharpoons Ag(111)/-SCH_2CH_3^{(\lambda-1)} + \lambda e^-} \quad (3)$$

Coulometric integration of the anodic branch of waves A and B (combined) yields a surface charge density of 72 ± 4 $\mu C/cm^2$ associated with $CH_3CH_2S^-$ deposition (after correction for

(15) (a) Tuschel, D. D.; Pemberton, J. E.; Cook, J. E. *Langmuir* **1986**, *2*, 380. (b) Tuschel, D. D.; Pemberton, J. E. *Langmuir* **1988**, *4*, 58.

(16) Ward, M. D. *J. Phys. Chem.* **1988**, *92*, 2049.

(17) Zeglinski, D. M.; Ogletree, D. F.; Beebe, T. P.; Hwang, R. O.; Somorjai, G. A.; Salmeron, M. B. *Rev. Sci. Instrum.* **1990,** *61*, 3769.

(18) (a) Wiechers, J.; Twomey, T.; Kolb, D. M.; Behm, R. J. *J. Electroanal. Chem.* **1988**, *248*, 451. (b) Nagahara, L. H.; Thundat, T.; Linsay, L. M. *Rev. Sci. Instrum.* **1989**, *60*, 3129.

(19) Lacy, W. B.; Williams, J. M.; Wenzler, L. A.; Beebe, T. P., Jr.; Harris, J. M. *Anal. Chem.* **1996**, *68*, 1003.

(20) Previous studies (Wall, D. J.; Bohn, P. W. *J. Phys. Chem.* **1990**, *94*, 2039) have demonstrated that strong in-plane depolarization of Raman scattering by SERS substrates interferes with the use of polarized scattering to determine molecular orientations; this limitation can be overcome and molecular orientations determined when the scattering intensity can be measured as a function of the refractive index of the overlaying solvent (Carron, K. T.; Hurley, L. G. *J. Phys. Chem.* **1991**, *95*, 9979).

(21) Pervin, D. D.; Sargent, E. P. *pK$_a$: Predictions For Organic Acids and Bases;* Chapman and Hall: New York, 1981; p 27.

(22) Bard, A. J.; Faulkner, L. R. *Electrochemical Methods: Fundamentals and Applications*; John Wiley and Sons: New York, 1980; p 522.

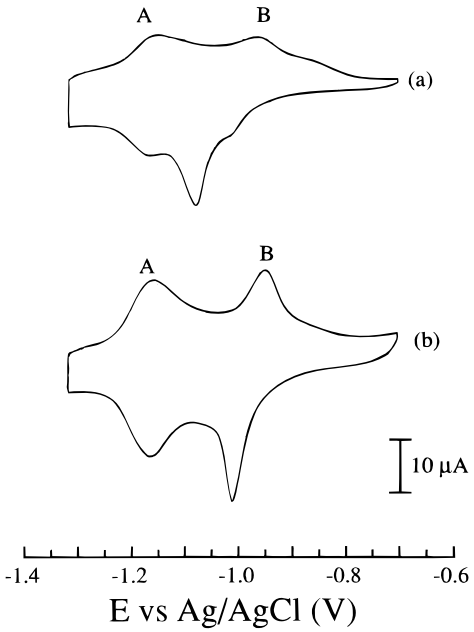

Figure 2. Voltammetric response of (a) an unannealed Ag electrode (area = 0.33 cm^2) in a 0.2 M NaOH solution containing 5 mM $CH_3CH_2S^-$. (b) Voltammetric response after annealing the same electrode in a H_2-air flame. Scan rate = 100 mV/s.

the electrode roughness (*vide infra*) and subtraction of the double layer charging current measured in solutions containing only 0.2 M NaOH). This value is in good agreement with charge densities previously measured by Porter and co-workers (∼68 $\mu C/cm^2$) for the reductive desorption of alkanethiolate monolayers from Ag(111) electrodes in basic ethanolic solutions.[23] Assuming that one electron is transferred per molecule of $CH_3CH_2S^-$ during oxidative adsorption (i.e., $n = 1$) and a $\sqrt{3} \times \sqrt{3}$/R30° monolayer structure (i.e., $\theta = 0.33$), the theoretical charge density anticipated for deposition of a complete $CH_3CH_2S^-$ monolayer is ∼73 $\mu C/cm^2$. We demonstrate below, from the measured dependency of $E_{1/2}$ on the bulk solution concentration of $CH_3CH_2S^-$, that n is indeed equal to ∼1. As noted in the Introduction, n includes charge resulting from physical processes in addition to the charge transferred (λ) in forming the Ag−S bond. Thus, employing a value of $n = 1$ does not necessarily imply that $\lambda = 1$ in eq 3.

The ability to cleanly resolve two voltammetric waves during $CH_3CH_2S^-$ deposition is strongly dependent on the thermal annealing of the Ag (111) electrode. For example, Figure 2a shows the voltammetric response of an unannealed Ag(111) electrode. Waves A and B are less well defined and a third poorly resolved oxidation/reduction wave is apparent. The response of the unannealed Ag electrode in Figure 2a is also characteristic of polycrystalline Ag electrodes, reflecting a strong dependency of the energetics and kinetics of oxidative adsorption on the orientation, roughness, and defect density of the Ag substrate. Heating the unannealed Ag electrode in a H_2 flame for several seconds yields a voltammetric response (Figure 2b) that is nearly identical to that of Ag(111) electrodes annealed in vacuum (Figure 1). Porter and co-workers have reported a similar dependence of the voltammetric response on surface preparation for reductive desorption of alkanethiolates from Au(111) and have ascribed the appearance of multiple peaks to desorption from terraces and step edge sites.[24] However, we believe that the two-wave voltammetric pattern observed at thermally annealed Ag(111) electrodes (Figure 1) reflects an inherent multistep and coverage-dependent structural ordering of the $CH_3CH_2S^-$ monolayer during oxidative adsorption. This point is discussed below in more detail.

Figure 3 shows *in-situ* STM images of unannealed and 6 h annealed Ag(111) films, recorded under potential control in 0.1 M NaF.[25] The images of the annealed and unannealed electrodes appear qualitatively similar, displaying channels (∼4 nm wide) and holes (∼2 nm diameter) at the surface of the 350 nm thick Ag films. Both surfaces exhibit atomically flat terraces, islands, and monoatomic steps of ∼3 Å height. The primary difference between the surface topographies is the presence of a significantly larger number of holes (compare Figures 3a and c), as well as smaller steps and islands, on the surface of the unannealed Ag films. Cross-sectional topographical profiles, shown in Figure 4 (corresponding to measurements along the diagonals of the images shown in Figure 3), allow a clearer visualization of the differences in the surface features of the unannealed and annealed films. From inspection of these profiles, it is apparent that the surface of the unannealed film is significantly rougher, exhibiting a larger periodic roughness (reflecting the larger density of holes) and a higher density of 1- and 2-atom high steps. In contrast, the profile of the 6 h annealed films suggests that these surfaces are atomically smooth over distances ranging from 100 to 200 nm. The key conclusion obtained from the STM data is that the decrease in surface roughness is associated with a significant improvement in the resolution of the two-wave voltammetric response. This finding suggests that the two-wave response (Figure 1) reflects the inherent mechanism of monolayer formation on Ag(111), rather than differences in the energetics of adsorption at specific surface sites (terraces vs steps).

Surface roughness factors (RF = electrochemically active (real) area/geometrical area) of the Ag films were estimated from cross-sectional STM line plots, such as the ones shown in Figure 4, by dividing the topographical profile length by the length of the straight cursor drawn across the image diagonal and squaring this value.[24,26] RF values measured by this procedure (estimated from nine independent measurements of 100 × 100 nm^2 STM images of annealed and unannealed films) were 1.06 ± 0.03 and 1.14 ± 0.04 for the 6 h annealed and unannealed Ag(111) films, respectively. These results agree within their uncertainties with the RF values determined by coulometric measurement (see Experimental Section) of the charge passed during the underpotential deposition (upd) of Pb monolayers, 1.02 ± 0.04 and 1.16 ± 0.06, respectively, for the 6 h annealed and unannealed Ag(111) films. The agreement between STM-based and Pb-upd-based RF values suggests that the STM images provide a relatively accurate measurement of the true electrochemically active area. Throughout this paper, we employ a RF value of 1.04 to correct the experimental coulometric charge densities for the residual surface roughness of the thermally annealed electrodes.

(23) Windrig, C. A.; Chung, C.; Porter, M. D. *J. Electroanal. Chem.* **1991**, *310*, 335.

(24) Walczak, M. M.; Alves, C. A.; Lamp, B. D.; Porter, M. D. *J. Electroanal. Chem.* **1995**, *396*, 103.

(25) We find that imaging the Ag surfaces in air is significantly more difficult than corresponding measurements of Au and Pt samples. This difficulty most likely results from the spontaneous formation of a surface Ag_xO layer in air or by adsorption of airborne contaminants. However, imaging the Ag films under potential control greatly enhances the resolution. Near atomic resolution was obtained for the Ag films in 0.1 M NaF solutions at potentials between −1.30 and −0.30 V vs Ag/AgCl.

(26) The STM images were acquired with 512 × 512 sampling resolution. In order to obtain a more accurate comparision between the STM- and electrochemically-based RF values, the same surface length scale should be used. For instance, for the upd of Pb, each Pb probes a 0.3 nm distance (the diameter of a Pb atom). Therefore, only STM images of 150 × 150 nm^2 or smaller (150 nm/512 pts = 0.3 nm pt^{-1}) should be used to determine the apparent RF. Analysis of larger STM images underestimate the RF since the local topography has been undersampled.

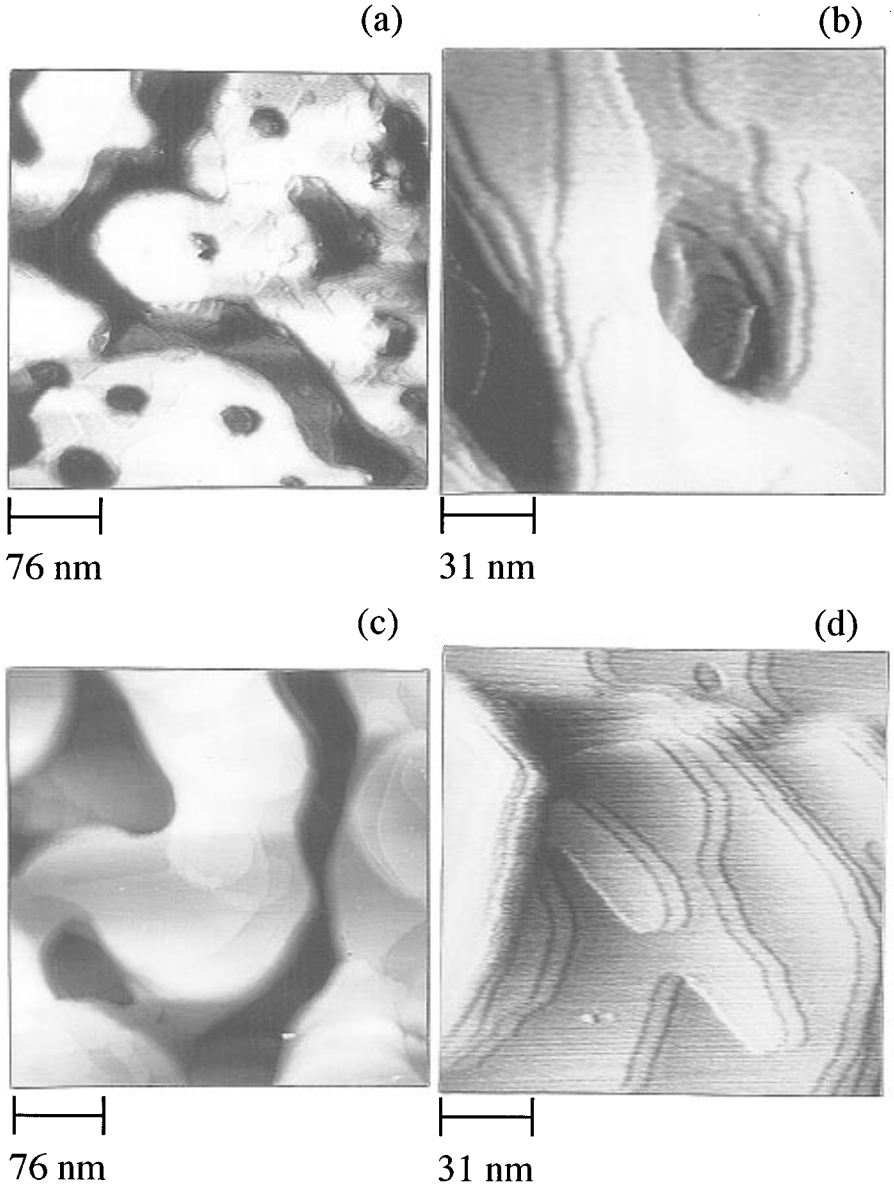

Figure 3. *In-situ* STM images of Ag films under potential control in 0.1 M NaF. The constant current images are slope subtracted to remove drift, but are otherwise unfiltered: (a) 350 × 350 nm^2 image of an unannealed film (tip−substrate bias (V_b) = −106 mV; tunneling current (i_t) = 2.2 nA); electrode potential vs Ag wire (E = −0.7 V); (b) 150 × 150 nm^2 image of an unannealed film (V_b = −107 mV; i_t = 2.2 nA; E = −0.7 V); (c) 350 × 350 nm^2 image of a 6 h annealed film (V_b = −94 mV; i_t = 1.9 nA; E = −1.3 V); (d) 150 × 150 nm^2 image of a 6 h annealed film (V_b = −94 mV; i_t = 1.9 nA, E = −0.7 V).

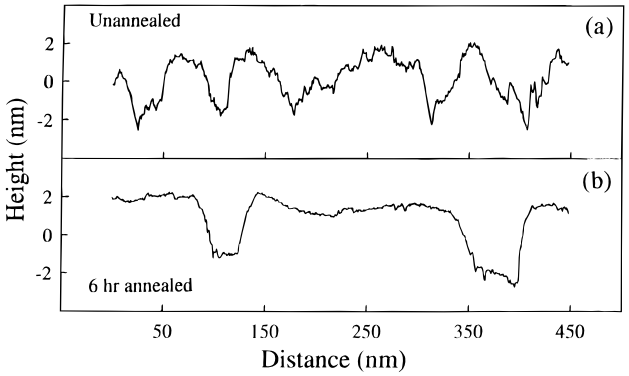

Figure 4. Cross-sectional STM line plots of (a) unannealed and (b) 6 h annealed Ag(111) films deposited on mica. Profiles obtained from images recorded under potential control in 0.1 M NaF.

Potential-Dependent Adsorption Isotherm. Surface-enhanced Raman spectroscopy (SERS) was used to monitor the potential-dependent adsorption of $CH_3CH_2S^-$ during voltammetric measurements. Both annealed and unannealed Ag(111) films used in this study are smooth in comparison to ORC-roughened polycrystalline Ag electrodes generally employed in SERS experiments.[27,28] However, we find that the *unannealed* Ag electrodes are sufficiently rough to allow a modest enhancement of the Raman intensity associated with adsorbed $CH_3CH_2S^-$. *In-situ* and *ex-situ* SERS spectra of the 6 h thermally annealed Ag(111) electrodes following deposition of a $CH_3CH_2S^-$ monolayer were featureless in the same wavenumber range, indicating that these surfaces are insufficiently rough to enhance the Raman intensity above background scattering levels.

The SERS spectral region investigated (600−750 cm^{-1}) covers the range of frequencies previously reported for the ν(C−S) stretching modes of the trans (∼710 cm^{-1}) and gauche (∼630 cm^{-1}) conformers of longer-chain alkanethiols (i.e.,

(27) The RF for a polycrystalline Ag disk was found to increase from ca. 1.3 to 2.5 after 15 oxidation−reduction cycles in 0.1 M KCl.

(28) Pemberton, J. E.; Guy, A. L.; Sobocinski, R. L.; Tuschel, D. D.; Cross, N. A. *Appl. Surf. Sci.* **1988**, *32*, 33.

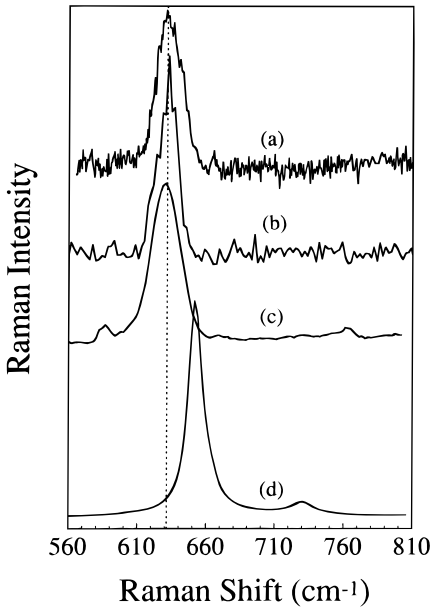

Figure 5. (a) *In-situ* SERS spectrum of an ORC-roughened polycrystalline Ag disk electrode in a 0.2 M NaOH solution containing 5 mM $CH_3CH_2S^-$ ($E = -0.78$ V vs Ag/AgCl). Integration time = 60 s. (b) Average of 10 *in-situ* SERS spectra obtained for an unannealed mica/Ag electrode under the same electrochemical and solution conditions as in part a. Integration time for each individual spectra = 60 s. (c) SERS spectrum of an $CH_3CH_2S^-$ monolayer deposited at open circuit on an ORC-roughened mica/Ag electrode. (d) Raman spectrum of neat ethanethiol. Integration time = 500 ms.

alkane chain lengths $n_c > 3$) self-assembled on Ag.[29] Figure 5a,b shows *in-situ* SERS spectra recorded within the ν(C−S) stretching region for an ORC-roughened polycrystalline Ag disk and an unannealed Ag(111) film. Both spectra were obtained with the electrodes immersed in a 0.2 M NaOH solution containing 5 mM $CH_3CH_2S^-$ at −0.78 V vs Ag/AgCl, sufficiently positive of wave B to ensure deposition of a complete monolayer. The center frequency of the ν(C−S) stretch for the *in-situ* SERS spectra is 632 cm^{-1}. Figure 5c shows the SERS spectrum of an ORC-roughened Ag(111) film on which an $CH_3CH_2S^-$ monolayer was deposited in an O_2-purged solution at open circuit. The ν(C−S) stretch occurs at the same frequency as that observed for the monolayer deposited under active potential control (Figure 5a,b). The Raman spectrum of neat ethanethiol (Figure 5d) displays a ν(C−S) stretch *ca.* 28 cm^{-1} higher than the surface-bound $CH_3CH_2S^-$.[30]

In-situ SERS spectra obtained at the polycrystalline Ag disk over the potential range encompassing waves A and B in for $CH_3CH_2S^-$ adsorption are presented in Figure 6. Figure 6a shows spectra obtained while stepping the potential in the positive direction, corresponding to adsorption; Figure 6b shows spectra obtained while stepping the potential in negative direction, corresponding to desorption. Spectra were recorded after the current decayed to background values (<1 s). SERS peak intensities extracted from the spectra, and the voltammogram recorded at the polycrystalline Ag disk used in the SERS experiment, are presented in Figure 7. The results clearly indicate that $CH_3CH_2S^-$ is completely desorbed from the Ag surface at potentials negative of wave A, a conclusion employed below in developing a thermodynamic analysis of half-wave potentials. The increase in SERS peak intensity is continuous

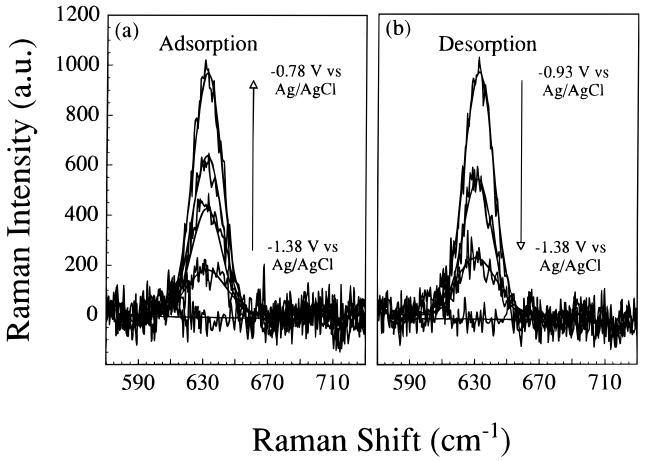

Figure 6. *In-situ* SERS spectra of the ν(C−S) stretch region (raw data and fitted data shown) for the (a) adsorption and (b) desorption of $CH_3CH_2S^-$ at an ORC-roughened polycrystalline Ag electrode in a 0.2 M NaOH solution containing 5 mM $CH_3CH_2S^-$. Applied potentials in (a) (from bottom to top) −1.38, −1.23, −1.13, −1.08, and −0.78 V, respectively, and in (b) (from top to bottom) −0.93, −1.18, −1.28, and −1.38 V, respectively. Integration time = 60 s.

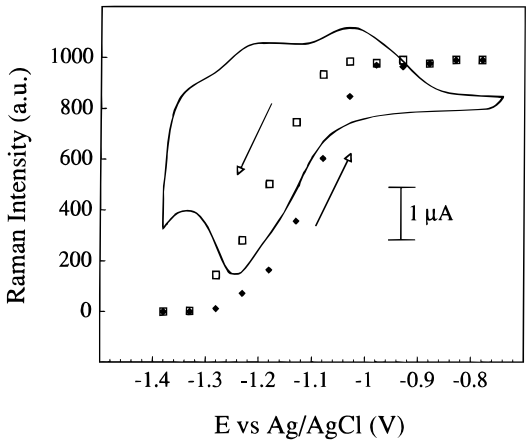

Figure 7. Voltammetric response and SERS intensity (integration time for each data point = 60 s) data obtained using a ORC-roughened polycrystalline Ag electrode (area = 3.5×10^{-2} cm^2) in a 0.2 M NaOH solution containing 5 mM $CH_3CH_2S^-$. The filled diamonds represent SERS intensities recorded during the adsorption of $CH_3CH_2S^-$ at 50 mV intervals. The open squares represent SERS intensities recorded during the desorption of $CH_3CH_2S^-$ over the same applied potential range. Scan rate = 100 mV/s.

over the potential range encompassing waves A and B, indicating that both waves are associated with oxidative adsorption.

(29) (a) Bryant, M. A.; Pemberton, J. E. *J. Am. Chem. Soc.* **1991**, *113*, 3629. (b) Joo, T. H.; Kim, K.; Kim, M. S. *J. Mol. Struct.* **1987**, *158*, 265. (c) Joo, T. H.; Kim, K.; Kim, M. S. *J. Phys. Chem.* **1986**, *90*, 5816. (d) Sandroff, C. J.; Garoff, S.; Leung, K. P. *Chem. Phys. Lett.* **1983**, *96*, 547.

(30) *In-situ* SERS spectra at frequencies between 1000 and 1310 cm^{-1} were also recorded during $CH_3CH_2S^-$ adsorption (same conditions as in Figure 5a). The SERS spectrum at electrode potentials positive of wave B displayed two bands centered at 1045 and 1250 cm^{-1}, in agreement with the spectrum reported by Joo et al. for $CH_3CH_2S^-$ adsorbed on Ag colloids.[29b] Both bands decreased to background levels when $CH_3CH_2S^-$ was desorbed at potentials negative of wave A. On the basis of SERS data reported by Bryant and Pemberton[29a] for alkanethiol monolayers on Ag, we assigned these two bands to the ν(C−C) stretching mode and the CH_2 wag, respectively. Both bands are also observed in the Raman spectrum of neat CH_3CH_2SH. The possibility of the oxidation of ethanethiolate to a sulfonate or sulfinate was explored by examining the SERS spectrum for ν(S−O) bands between 1000 and 1250 cm^{-1} (Lin-Vien, D.; Colthup, N. B.; Fateley, W. G.; Graselli, J. G. *Infrared and Raman Characteristic Frequencies of Organic Molecules*; Academic Press: San Diego, CA, 1991; Chapter 14). No SERS bands, other than the 1045 and 1250 cm^{-1} bands noted above, were observed in this frequency range, indicating that the $CH_3CH_2S^-$ monolayer is stable at negative potentials (<−0.7 V vs Ag/AgCl) in O_2-purged solutions.

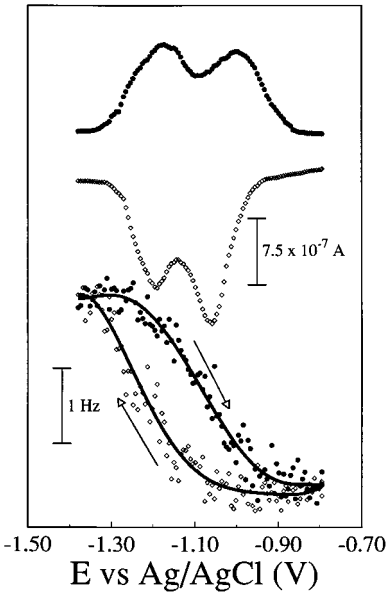

Figure 8. Voltammetric and frequency response of an Ag-coated quartz crystal microbalance in a 0.2 M NaOH solution containing 5 mM $CH_3CH_2S^-$. Scan rate = 10 mV/s. Filled circles represent adsorption of the $CH_3CH_2S^-$ monolayer. Open diamonds represent desorption of the $CH_3CH_2S^-$ monolayer.

The potential-dependent adsorption isotherm was quantitatively determined by measuring the mass deposited on the Ag(111) surface using a 5 MHz electrochemical quartz crystal microbalance (EQCM). Measurements were made using a quartz crystal onto which Ag electrodes were thermally deposited and annealed in vacuum.[11a] Figure 8 shows the voltammetric and frequency response (obtained simultaneously) for an Ag-coated quartz crystal in contact with a 0.2 M NaOH solution containing 5 mM $CH_3CH_2S^-$. A reversible 2.8 ± 0.4 Hz decrease in the EQCM frequency response is observed upon scanning the electrode potential in the positive direction through waves A and B, corresponding to an increase in the surface mass associated with $CH_3CH_2S^-$ adsorption.

The Sauerbrey equation[31] (eq 4) allows the frequency response of the EQCM, Δf, to be quantitatively related to the interfacial mass change, Δm.

$$\Delta f = -2f_o^2 \Delta m / A(\mu_q \rho_q)^{1/2} \quad (4)$$

In eq 4, f_o is the parent resonant frequency of the crystal ($\sim 5 \times 10^6$ Hz), A is the area of shear motion (0.178 cm^2), and μ_q and ρ_q are the shear modulus (2.947×10^{11} g cm^{-1} s^{-2}) and density (2.648 g cm^{-3}) of quartz, respectively. Using these values, the observed 2.8 ± 0.4 Hz frequency shift corresponds to a surface concentration of $\Gamma = 8.1 \pm 1.2 \times 10^{-10}$ mol/cm^2. Coulometric integration of the voltammetric waves measured during the EQCM experiment (Figure 8) yields a surface concentration of $\Gamma = 7.2 \times 10^{-10}$ mol/cm^2, assuming $n = 1$ as described previously.

Combined, the SERS, EQCM, and voltammetric data indicate that waves A and B of the voltammetric response (Figure 1) correspond to oxidative adsorption of $CH_3CH_2S^-$. Scheme 1 depicts a proposed mechanism of this two-step process, which is further supported by experiments to be described below. In proposing this mechanism, the SERS data are important in demonstrating that $CH_3CH_2S^-$ is not adsorbed at Ag(111) at potentials negative of wave A. Thus, oxidative adsorption, rather than physisorption, is the primary mechanism responsible for the increased surface coverage of $CH_3CH_2S^-$. Although this has been assumed in previous studies, we are not aware of a similar experimental demonstration that the metal is essentially free of alkanethiolates at negative potentials.

(31) Sauerbrey, G. *Z. Phys.* **1959**, *155*, 206.

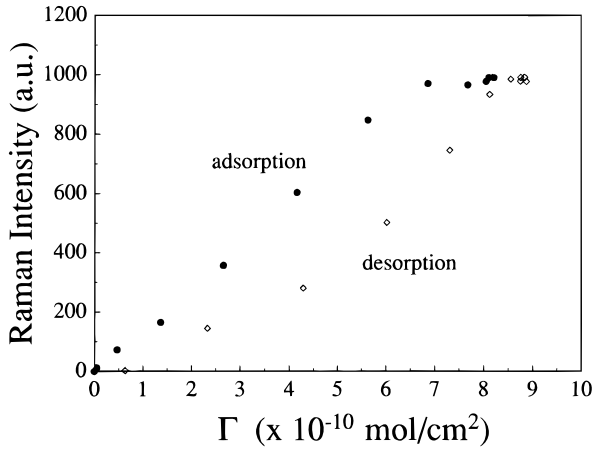

Figure 9. Plot of Raman intensity vs EQCM-measured surface concentration (data from Figures 7 and 8).

Scheme 1

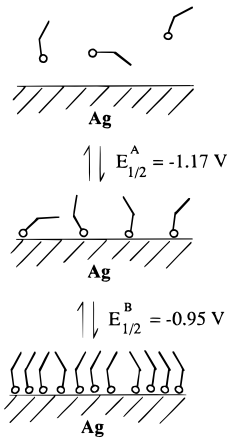

The EQCM-based adsorption isotherm, as well as the potential dependency of the SERS intensity, indicate that both wave A and wave B correspond to $CH_3CH_2S^-$ adsorption. Figure 9 displays the Raman intensity as a function of the EQCM-determined surface coverage, where each point corresponds to a surface coverage and Raman intensity obtained at the same applied potential. As shown in Figure 9, the Raman intensity is proportional to the surface coverage during adsorption of $CH_3CH_2S^-$ and levels out at a surface coverage corresponding to $\sim$80% of a monolayer. This behavior is very similar to the surface coverage-dependent SERS intensity measured in a recent surface-dosing study of SERS enhancement,[32] as well an earlier electrochemical study of pyridine SERS scattering where the voltammetric response was used to estimate the surface coverage.[33] Since the SERS intensity is proportional to the surface coverage of $CH_3CH_2S^-$ for all but the highest coverages, the plot of SERS intensity vs electrode potential (Figure 7) may be regarded as the potential-dependent isotherm for adsorption of $CH_3CH_2S^-$. Data obtained during oxidative adsorption (on the positive-going potential scan) verify this assertion with good linearity between the SERS intensity and EQCM-based surface coverages (Figure 9) whereas data obtained during reductive desorption show less clear agreement.

(32) Lacy, W. B. Ph.D. Thesis, University of Utah, 1996.

(33) Stolberg, L; Lipkowski, J.; Irish, D. E. *J. Electroanal. Chem.* **1991**, *300*, 563.

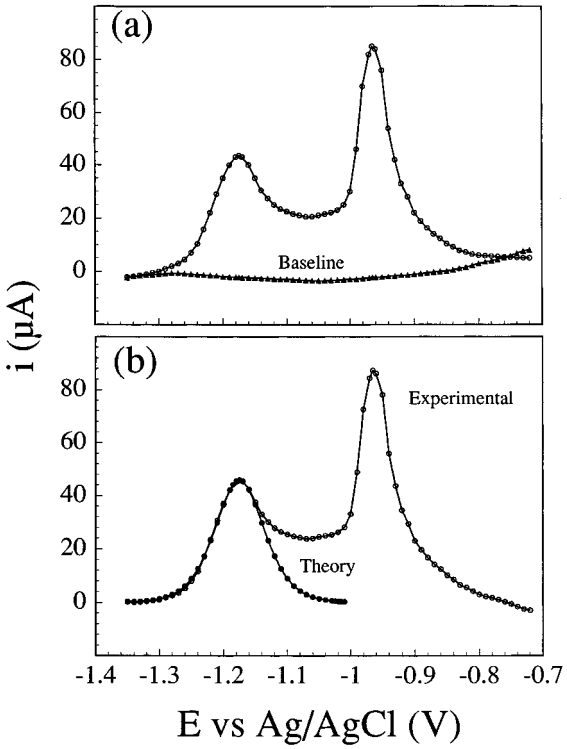

Figure 10. (a) Positive-going scan of the voltammetric response of a 2.0 cm^2 Ag(111) electrode immersed in a solution containing 5 mM $CH_3CH_2S^-$ and 0.2 M NaOH. The base line current was recorded using the same electrode in a 0.2 M NaOH solution in the absence of $CH_3CH_2S^-$. (b) Comparison of the base-line-subtracted voltammogram (from part a) with the theoretical voltammetric response of an electrode covered by an electroactive monolayer (eq 5). The theoretical response is computed assuming a thermodynamically reversible redox system and the following parameters: $T = 298$ K, $\nu = 0.1$ V/s, $n = 1$, $A = 2.0$ cm^2, $\Gamma^* = 2.44 \times 10^{-10}$ mol/cm^2, and $E_{1/2} = -1.17$ V vs Ag/AgCl.

This difference can be rationalized by noting that the anodic waves of the voltammetric curves recorded using the polycrystalline Ag electrode (on which the *in-situ* SERS data were acquired) and the Ag-coated quartz crystal (employed in the EQCM measurement) are nearly identical, indicating that adsorption of $CH_3CH_2S^-$ has a similar potential dependence on both substrates. However, the cathodic desorption waves are significantly broader and less well resolved at the polycrystalline Ag electrode than at the Ag-coated quartz crystal. Thus, the deviation of the SERS and EQCM data during desorption is likely due to the substrate-based differences in the potential dependence of this process.

Electrosorption Valency. As noted previously, the symmetrical shape of wave A indicates that the initial oxidative adsorption of $CH_3CH_2S^-$ at Ag(111) is a thermodynamically reversible process. In Figure 10a, the anodic peaks of waves A and B are shown, along with the background current measured for the same Ag(111) electrode in a solution containing only 0.2 M NaOH (after reductive desorption of $CH_3CH_2S^-$ to produce a bare surface). The background-subtracted voltammogram is replotted in Figure 10b and compared to the theoretical voltammetric response anticipated for a reversible redox surface process, (eq 5), assuming a Langmuir adsorption isotherm for both reduced and oxidized forms of the surface adsorbate.[22]

$$i = \frac{n^2F^2}{RT}\frac{\nu A\Gamma^* \exp[(nF/RT)(E - E_{1/2})]}{\{1 + \exp[(nF/RT)(E - E_{1/2})]\}^2} \qquad (5)$$

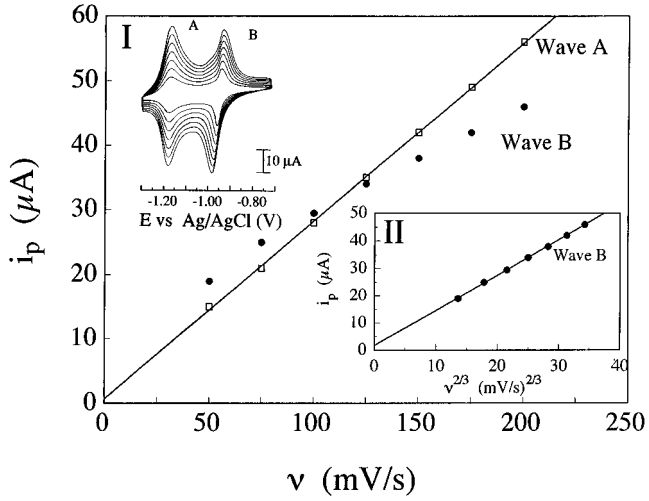

Figure 11. Dependence of the anodic peak currents (i_p) on the voltammetric scan rate (ν) for an annealed Ag(111) electrode (area = 0.32 cm^2) in a 0.2 M NaOH solution containing 5 mM $CH_3CH_2S^-$. Wave A open squares; wave B filled circles. Inset I: raw voltammetric data. Inset II: i_p plotted vs $\nu^{2/3}$ for wave B.

In eq 5, ν is the voltammetric scan rate, Γ^* is the total surface coverage of the adsorbate associated with wave A, and A is the electrode area. A theoretical voltammogram computed using eq 5 is compared to the experimental voltammogram using $n = 1$ and $\Gamma^* = 2.44 \times 10^{-10}$ mol/cm^2, where Γ^* represents the maximum surface coverage associated with wave A. All other parameters used in computing the theoretical response are measured ($T = 298$ K, $\nu = 0.1$ V/s, $A = 2.0$ cm^2, and $E_{1/2} = -1.17$ V vs Ag/AgCl). Inspection of Figure 10b shows that relatively good agreement is obtained between the theoretical (eq 5) and experimental voltammograms except at potentials significantly positive of $E_{1/2}$.

The shape of the theoretical voltammogram is particularly sensitive to the value of n employed in eq 5. For instance, using $n = 0.75$ yields a voltammetric wave that is ca. 33% broader than the curve shown in Figure 10b. Thus, the relatively good fit of eq 5 to the experimental results provides preliminary evidence that approximately one electron is transferred per molecule during electrodeposition of $CH_3CH_2S^-$ at potentials corresponding to wave A.

The agreement between the theoretical and experimental voltammetric curves indicates that the initial adsorption of $CH_3CH_2S^-$ is rapid on voltammetric time scales and that minimal lateral interactions exist with the adsorbed layer at low coverages. At higher surface coverages, corresponding to potentials positive of $E_{1/2}$, the agreement between theory and experiment is poor, undoubtedly reflecting a departure from the assumption of noninteracting adsorbates. The reversibility of wave A is also demonstrated in the dependence of peak currents (i_p) on the voltammetric scan rate (ν) Figure 11. We observe that i_p for wave A is proportional to ν (both anodic and cathodic peak currents) for $50 < \nu < 200$ mV/s. Over the same range of ν, the peak splitting (ΔE_p) between cathodic and anodic waves increases by a negligible amount (Inset I of Figure 11), indicating that the kinetics of adsorption/desorption are immeasurably fast on the time scale of the voltammetric experiments. In contrast, for wave B, the i_p vs ν plot is nonlinear, and ΔE_p increases significantly with ν; both dependencies indicate a kinetically slow surface redox process. The voltammetric peak currents for wave B are proportional to $\nu^{2/3}$ (Inset II of Figure 11), a scan rate dependency that is characteristic of

nucleation and growth of ordered surface phases.[34] Thus, the scan rate dependencies indicate that adsorption/desorption of $CH_3CH_2S^-$ is rapid at low coverages (wave A), but proceeds at a much slower rate with increasing coverage (wave B). We speculate that the kinetic limitation associated with wave B results from structural ordering of the monolayer at higher coverage, necessary in order to accommodate a more densely packed monolayer. In this respect, the mechanism proposed in Scheme 1 is analogous to that directly observed by Poirier and Pylant for the self-assembly of alkanethiols on Au(111) from the vapor phase.[6a]

The thermodynamic reversibility of wave A suggests that a value of *n* may be determined by measuring the dependency of $E_{1/2}$ on the bulk concentration of $CH_3CH_2S^-$. In order to relate $E_{1/2}$ to $[CH_3CH_2S^-]$, we recast the overall reaction for oxidative adsorption (eq 3) in terms of the adsorption pre-equilibrium and electron transfer steps

$$CH_3CH_2S^- + Ag(111) \underset{k_d}{\overset{k_a}{\rightleftharpoons}} Ag(111)(CH_3CH_2S^-)_{ads} \quad (6)$$

$$Ag(111)(CH_3CH_2S^-)_{ads} \overset{E^{\circ\prime}}{\rightleftharpoons} Ag(111)/-SCH_2CH_3^{(\lambda-1)} + \lambda e^- \quad (7a)$$

where $Ag(111)(CH_3CH_2S^-)_{ads}$ represents $CH_3CH_2S^-$ *physisorbed* on the Ag(111) surface prior to charge transfer step.

Although the generation of electrical charge is explicitly expressed by eq 7a, the adsorption preequilibrium (eq 6) will also result in a measurable current, a consequence of the movement of the charged species $CH_3CH_2S^-$ through the electric field at the metal/solution interface.[35] As discussed above, this nonfaradaic process, as well as others such as interactions of the adsorbate and solvent dipoles with the electric field, also generates measurable currents.[36,37] Thus, the total charge *n* resulting in deposition of one molecule of $CH_3CH_2S^-$ is the sum of these individual contributions. Although *n* includes nonfaradaic processes, all contributions to *n* effect the chemical potential of the adsorbate. Thus, in order to develop a thermodynamic analysis that reflects the influence of *n*, eq 7a is rewritten as

$$(-\nu_R)Ag(111)(CH_3CH_2S^-)_{ads} \overset{E^{\circ\prime}}{\rightleftharpoons} (\nu_O)Ag(111)/-SCH_2CH_3 + ne^- \quad (7b)$$

where ν_R (=−1) and ν_O (=+1) are stoichiometric coefficients.

Whereas eq 7a represents the faradaic reaction and degree of charge transferred in forming the Ag−S surface bond, eq 7b expresses the overall electrical charge generated during adsorption of $CH_3CH_2S^-$ and, thus, correctly indicates the influence of the electric potential on the surface activities of Ag(111)-$(CH_3CH_2S^-)_{ads}$ and Ag(111)/−SCH_2CH_3.[38] Therefore, eq 7b is the expression employed in developing the Nernst relationship described below.

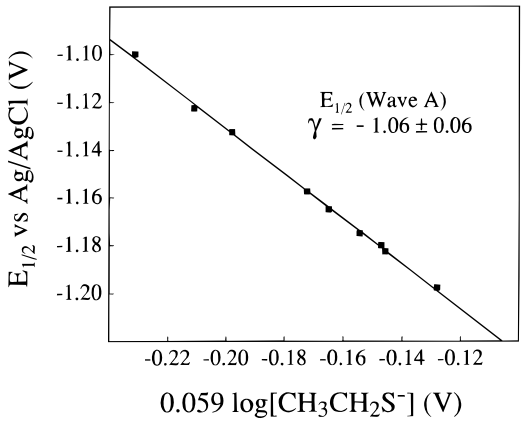

Figure 12. Plot of $E_{1/2}$ for wave A as a function of the bulk solution concentration of $CH_3CH_2S^-$. The value of γ indicated on the plot is equal to the inverse slope of the line (see eq 10 of the text).

In-situ SERS measurements indicate that the adsorption pre-equilibrium (eq 6) lies far to the left (i.e., $k_d \gg k_a$). The fact that wave A is reversible indicates that both eqs 6 and 7b are also reversible; thus, the Nernst relationship for this system (see Appendix) is given by

$$E = E_{1/2} + \frac{RT}{nF}\ln(\theta_o^{\nu_o}(1-\theta_o)^{\nu_R}) \quad (8)$$

where

$$E_{1/2} = E^{\circ\prime} + \frac{RT}{nF}\ln\left(\frac{\beta[CH_3CH_2S^-]}{1+\beta[CH_3CH_2S^-]}\right)^{\nu_R} \quad (9)$$

In eqs 8 and 9, $\theta_o = \Gamma/\Gamma^*$, $\beta = k_a/k_d$, and $E_{1/2}$ corresponds to the electrode potential where $\theta_o = {}^1/_2$. Since the *in-situ* SERS results indicate that $\beta \ll 1$ and because $[CH_3CH_2S^-] \ll 1$ for all solution conditions, eq 9 can be simplified and rewritten at $T = 298$ K as the following:

$$E_{1/2} = E^{\circ\prime} + \frac{0.059}{n}\log(\beta[CH_3CH_2S^-])^{\nu_R} \quad (10)$$

Equation 10 indicates that a plot of $E_{1/2}$ vs $0.059\log[CH_3CH_2S^-]$ should be linear with a slope equal to $(n/\nu_R)^{-1}$. The quantity (n/ν_R) is defined as the electrosorption valency, γ, which clearly is a negative quantity for oxidative adsorption of anions (where *n* is positive and ν_R is negative).[39] Figure 12 shows the corresponding plot of experimental values, from which a value of $\gamma = -1.06 \pm 0.06$ is obtained. Thus, for wave A, oxidative adsorption of $CH_3CH_2S^-$ on Ag(111) is indeed a one-electron process (i.e., $n \approx 1$ in eq 7b). Because the voltammetric behavior of wave B suggests a kinetically slow and more complex process, the preceding thermodynamic treatment can not be reliably applied to the analysis of this wave. However, we note that γ may vary as a function of surface coverage, especially at higher coverages where lateral interactions between molecules become more significant.[36,37,39]

As a tangential comment, the analysis based on eq 10 can be shown to be equivalent to the thermodynamic definition of γ originally presented by Vetter and Schultze[39]

(34) (a) Fletcher, S. J. *Electroanal. Chem.* **1981**, *118*, 419. (b) Maestre, M. S.; Rodriguez-Amaro, R.; Munoz, E.; Ruiz, J. J.; Camacho, L. *J. Electroanal. Chem.* **1994**, *373*, 31.

(35) Transport of an ion through the interfacial field contributes a fractional charge, *gz*, to the electrosorption valency, where *g* represents a normalized relative distance within the Helmholtz layer and *z* is the ion charge (−1 for ethanethiolate). See discussion in ref 39.

(36) (a) Schultze, J. W.; Koppitz, F. D. *Electrochim. Acta* **1976**, *21*, 327. (b) Koppitz, F. D.; Schultze, J. W. *Electrochim. Acta* **1976**, *21*, 337.

(37) Swathirajan, S.; Bruckenstein, S. *Electrochim. Acta* **1983**, *28*, 865.

(38) It should be clear that eq 7b is not a stoichiometric electrochemical reaction, but rather a representation of the quantity of electrical charge (*n*) generated during adsorption of one molecule. Equation 7b is sometimes incorrectly expressed in terms of the electrosorption valency, γ, instead of *n*. This usage of γ is inconsistent with the thermodynamic expression $(\partial\mu_i/\partial E)_{\mu_{j\neq i}} = \gamma F$ and leads to a sign error in the numerical value of γ. See ref 39 for a more thorough discussion of these relationships.

(39) (a) Vetter, K. J.; Schultze, J. W. *Ber. Bunsen-Ges. Phys. Chem.* **1972**, *76*, 920. (b) Vetter, K. J.; Schultze, J. W. *Ber. Bunsen-Ges. Phys. Chem.* **1972**, *76*, 927. (c) Schultze, J. W.; Vetter, K. J. *J. Electroanal. Chem.* **1973**, *44*, 63. (d) Vetter, K. J.; Schultze, J. W *J. Electroanal. Chem.* **1974**, *53*, 67.

$$\gamma = \frac{1}{F}\left(\frac{\partial \mu_{RS^-}}{\partial E}\right)_{\Gamma} \quad (11)$$

where $\mu_{RS}-$ is the chemical potential of the $CH_3CH_2S^-$ in the bulk solution. Substituting $\mu_{RS}- = \mu^{\circ}{}_{RS}- + RT \ln(a_{RS}-)$, where $a_{RS}-$ and $\mu^{\circ}{}_{RS}-$ are the activity and standard chemical potential of $CH_3CH_2S^-$, respectively, yields:

$$\gamma = \frac{1}{F}\left(\frac{\partial \mu_{RS^-}}{\partial E}\right)_{\Gamma} = \frac{1}{F}\left(\frac{\partial \mu_{RS^-}}{\partial E_{1/2}}\right) \approx \frac{RT}{F}\left(\frac{\partial(\ln[CH_3CH_2S^-])}{\partial E_{1/2}}\right) \quad (12)$$

The approximate sign in eq 12 indicates that solution activity effects are ignored (i.e., $a_{RS}- \approx [CH_3CH_2S^-]$). It can be easily shown that eq 10 is consistent with eq 12.

The value of γ determined above is based on the assumption of microscopic reversibility of eqs 6 and 7b. An independent estimate of γ which can be obtained from the expression

$$\gamma = -\frac{1}{F}\left(\frac{\partial q}{\partial \Gamma}\right)_{E} \quad (13)$$

where $(\partial q/\partial \Gamma)_E$ is the differential rate of charge passed during adsorption of the molecule, which, as before, includes contributions from both charge transfer (i.e., faradaic) and physical processes. (By definition, the current density measured during adsorption of $CH_3CH_2S^-$ is equal to $(\partial q/\partial t)_E$, where q is a positive quantity.) A straightforward estimate of γ may be obtained from the voltammetric experiments by assuming that $(\partial q/\partial \Gamma)_E$ is constant over the potential range where adsorption occurs. Employing this assumption yields:

$$\gamma = -\frac{Q}{F\Gamma^*} \quad (14)$$

where Q and Γ^* are the integrals of q and Γ measured over the same potential interval. Substituting the values of Q and Γ^* measured in the EQCM experiment described above (70 μC/cm^2 and 8.1×10^{-10} mol/cm, respectively, for waves A and B combined) yields $\gamma = -0.90 \pm 0.14$, within error of the value of γ determined above using the thermodynamic analysis (-1.06 ± 0.06). Thus, both methods indicate that the electrosorption valency is approximately equal to unity, justifying the earlier use of $n = 1$ in computing values of Γ^* from the coulometric charge measured in the voltammetric experiment ($\Gamma^* = Q/nF$). In addition, since the estimate of γ from the combined coulometric/EQCM measurement reflects the average electrosorption valency associated with waves A and B, whereas the dependency of $E_{1/2}$ on $[CH_3CH_2S^-]$ yields γ only for wave A, the finding that both methods yield the same value suggests that γ is essentially independent of the surface coverage and electrode potential.

Conclusion. We have demonstrated that oxidative adsorption of $CH_3CH_2S^-$ occurs through a two-step potential-dependent mechanism which, by definition, indicates that two energetically-distinct surface phases exist on Ag(111) during monolayer formation. The voltammetric behavior and coulometric results suggest that these phases correspond to a disordered, low-coverage phase in which the lateral interactions between molecules are minimal (wave A) and a more structurally ordered, high-coverage phase (wave B). A similar two-wave voltammetric response is observed for longer chain alkanethiolates ($n_c < 6$), which will be described in a forthcoming report detailing factors that influence the thermodynamic stability of monolayers formed on both Au(111) and Ag(111) surfaces.[12] The $E_{1/2}$ values reported here (-1.17 and -0.95 V vs Ag/AgCl) correspond to adsorption free energies of -22.4 and -17.4 kcal/mol, respectively, for the low (wave A) and high (wave B) coverage surface phases. The finding that $E_{1/2}$ for the lower coverage phase is more negative than that for the higher density phase indicates that the energetics of adsorption are controlled to a large extent by the energy associated with the formation of the Ag−S bond, rather than by cohesive lateral interactions between the adsorbed molecules. The situation may be different for longer chain alkanethiolates, where chain−chain interactions may dominate the overall free energy of adsorption.

Self-assembly of alkanethiol monolayers in solution under open circuit conditions (the most common procedure for monolayer deposition) corresponds to deposition at electrode potentials very positive of the $E_{1/2}$ values of waves A and B reported here. Thus, self-assembly is generally performed under conditions far from the equilibrium potential of adsorption. Although this is assumed throughout the literature, we are not aware of any previous statement of this conclusion supported by experimental data obtained under true equilibrium conditions. A similar conclusion is embodied in the reversible electrode potentials observed by Weisshaar, Lamp, and Porter for alkanethiolate deposition on Au(111).[9]

The Nernst expression derived here allows the electrosorption valency, γ, to be determined from the dependence of $E_{1/2}$ values on the bulk solution concentration. Application of this method depends on whether a reliable value of $E_{1/2}$, under equilibrium conditions, can be obtained from the voltammetric measurement. The value of γ determined here (~ -1) for $CH_3CH_2S^-$ adsorption on Ag(111) is the same as that previously determined for oxidative adsorption of HS^- at Ag(111),[11a] but larger than that determined by Schneider and Buttry for self-assembled long-chain ($n_c = 12$) alkanethiol films on Au(111), $\gamma \approx -0.5$.[10a] It is most likely that the coefficient λ, describing the degree of charge transferred from the molecule to the metal surface, is larger at Ag(111) than that for Au(111), possibly accounting for part of the difference in γ values for the alkanethiolate monolayers on the different surfaces. However, the large difference in the chain lengths of the molecules employed in these studies, $n_c = 2$ vs $n_c = 12$, may result in significantly different interfacial charge distributions, as initially pointed out by Schneider and Buttry.[10a] This dependence of the charge distribution suggests that the nonfaradaic component of γ may also be a function of chain length. Thus, it is not possible, on the basis of the current experimental results, to unequivocally interpret the difference in our value of γ and that measured by Schneider and Buttry. We are currently investigating if γ is a function of chain length for alkanethiolate deposition on Ag(111).

Finally, the *in-situ* SERS results reported here represent the first direct experimental evidence that alkanethiolates are completely desorbed from the metal surface upon reductive desorption in aqueous solutions. This finding is not only important in the thermodynamic analysis of $E_{1/2}$ values but also provides a basis for computing *absolute* value of the surface coverage, Γ, from the EQCM measurement of the *relative* change in mass.

Acknowledgment. This research was supported by the Office of Naval Research; the SERS measurements were supported by a grant from the U.S. Department of Energy. H.S.W. gratefully acknowledges informative discussions with D. A. Buttry (University of Wyoming) and Debra Rolison (Naval Research Laboratory) and preprints of unpublished work from M. D. Porter (Iowa State University) and I. Fritsch (University of Arkansas).

Appendix 1. Nernst Expression for Electrodeposited Alkanethiolate Films (eqs 8 and 9)

We consider the general mechanism,

$$R \underset{k_d}{\overset{k_a}{\rightleftharpoons}} R_{ads} \tag{A.1}$$

$$(-\nu_R)R_{ads} \overset{E^{\circ\prime}}{\rightleftharpoons} (\nu_O)O_{ads} + ne^- \tag{A.2}$$

describing the oxidative adsorption of species R, where ν_R and ν_O are stoichiometric coefficients. We adopt the standard convention that ν_R is negative and ν_O is positive. R is present in the bulk solution at concentration C_R* and is reversibly adsorbed to form R_{ads} (eq A.1), which is oxidized to O_{ads} at potentials positive of the formal redox potential, $E^{\circ\prime}$ (eq A.2). Equations A.1 and A.2 are analogous to eqs 6 and 7b in the text, which describe the oxidative adsorption of ethanethiolate.

The Nernst equation for the redox system, $\sum \nu_i X_i + ne^- = 0$, is written in terms of the surface concentrations Γ_O and Γ_R.

$$E = E^{\circ\prime} + (RT/nF)\ln(\Gamma_O{}^{\nu_O}\Gamma_R{}^{\nu_R}) \tag{A.3}$$

Assuming a Langmuir model of adsorption, the surface concentration of R_{ads} may be expressed in terms of the saturation surface concentration of R_{ads}, Γ_R*, and the rate constants for adsorption (k_a) and desorption (k_d).

$$\frac{d\Gamma_R}{dt} = k_a C_R^*(\Gamma_R^* - \Gamma_R - \Gamma_O) - k_d\Gamma_R \tag{A.4}$$

At equilibrium,

$$\Gamma_R = \frac{\beta C_R^*(\Gamma_R^* - \Gamma_O)}{1 + \beta C_R^*} \tag{A.5}$$

where $\beta \equiv k_a/k_d$. Substitution of eq A.5 into eq A.3 yields

$$E = E^{\circ\prime} + (RT/nF)\ln\left(\Gamma_O{}^{\nu_O}\left[\frac{(\Gamma_R^* - \Gamma_O)\beta C_R^*}{(1 + \beta C_R^*)}\right]^{\nu_R}\right) \tag{A.6}$$

For the special case where $-\nu_R = \nu_O$ and the saturation surface concentrations of O and R are approximately equal (i.e., $\Gamma_R^* = \Gamma_O^*$), eq A.6 can be rewritten in terms of the surface coverages, $\theta_O = \Gamma_O/\Gamma_O^*$ and $\theta_R = \Gamma_R/\Gamma_R^*$

$$E = E^{\circ\prime} + (RT/nF)\ln\left(\theta_O{}^{\nu_o}\left[\frac{(1 - \theta_O)\beta C_R^*}{(1 + \beta C_R^*)}\right]^{\nu_R}\right). \tag{A.7}$$

The half-wave potential, $E_{1/2}$, is defined as the potential as which $\theta_O = {}^1/_2$. Thus,

$$E = E_{1/2} + (RT/nF)\ln(\theta_O{}^{\nu_o}(1 - \theta_O)^{\nu_R}) \tag{A.9}$$

where

$$E_{1/2} = E^{\circ\prime} + (RT/nF)\ln\left[\frac{\beta C_R^*}{(1 + \beta C_R^*)}\right]^{\nu_R} \tag{A.10}$$

Substituting the definition of the electrosorption valency, $\gamma = (n/\nu_R)$, yields

$$E_{1/2} = E^{\circ\prime} + (RT/\gamma F)\ln\left[\frac{\beta C_R^*}{(1 + \beta C_R^*)}\right] \tag{A.11}$$

which is identical to eq 9 in the text.

JA964396J